

OccupancyDETR: Making Semantic Scene Completion as Straightforward as Object Detection*

Yupeng Jia^{1†}, Jie He^{2†}, Runze Chen³, Fang Zhao³ and Haiyong Luo^{4‡}

Abstract—Visual-based 3D semantic occupancy perception (also known as 3D semantic scene completion) is a new perception paradigm for robotic applications like autonomous driving. Compared with Bird’s Eye View (BEV) perception, it extends the vertical dimension, significantly enhancing the ability of robots to understand their surroundings. However, due to this very reason, the computational demand for current 3D semantic occupancy perception methods generally surpasses that of BEV perception methods and 2D perception methods. We propose a novel 3D semantic occupancy perception method, OccupancyDETR, which consists of a DETR-like object detection module and a 3D occupancy decoder module. The integration of object detection simplifies our method structurally - instead of predicting the semantics of each voxels, it identifies objects in the scene and their respective 3D occupancy grids. This speeds up our method, reduces required resources, and leverages object detection algorithm, giving our approach notable performance on small objects. We demonstrate the effectiveness of our proposed method on the SemanticKITTI dataset, showcasing an mIoU of 23 and a processing speed of 6 frames per second, thereby presenting a promising solution for real-time 3D semantic scene completion. Code is available at <https://github.com/jypjypjypjyp/OccupancyDETR>.

I. INTRODUCTION

3D semantic perception serves as a fundamental capability for robotics. The prevalent approach currently employs multi-sensor fusion involving LiDAR and camera [1], [2], [3], which has achieved strong performance and resulted in numerous product implementations. However, this approach raises concerns such as high costs and lack of portability.

* This work was supported in part by the Strategic Priority Research Program of Chinese Academy of Sciences under Grant XDA28040500, the National Natural Science Foundation of China under Grant 62261042 and 62002026, the Key Research Projects of the Joint Research Fund for Beijing Natural Science Foundation and the Fengtai Rail Transit Frontier Research Joint Fund under Grant L221003, Beijing Natural Science Foundation under Grant 4212024 and 4222034, the Key Research and Development Project from Hebei Province under Grant 21310102D, the Fundamental Research Funds for the Central Universities under Grant 2022RC13, Yibin City Introduction of High-Level Talent Project under Grant 2022YG03 and the Open Project of the Beijing Key Laboratory of Mobile Computing and Pervasive Device, Institute of Computing Technology, Chinese Academy of Sciences (Corresponding author: Haiyong Luo)

¹ Yupeng Jia graduated from School of Computer Science (National Pilot Software Engineering School), Beijing University of Posts and Telecommunications, Beijing, China

² Jie He graduated from School of Computer Science (National Pilot Software Engineering School), Beijing University of Posts and Telecommunications, Beijing, China

³ School of Computer Science (National Pilot Software Engineering School), Beijing University of Posts and Telecommunications, Beijing, China

⁴ Institute of Computing Technology, Chinese Academy of Sciences, Beijing, China

[†] Equal contribution.

[‡] Corresponding author, email addresses: yhluo@ict.ac.cn

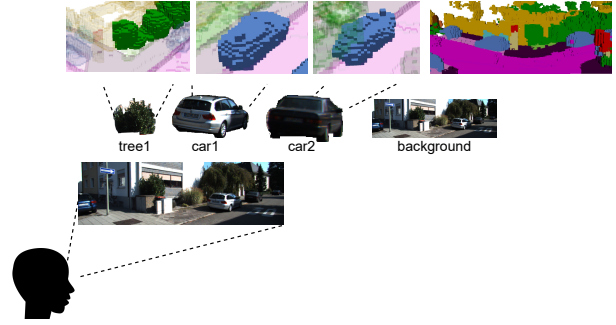


Fig. 1. Concept diagram of 3D semantic occupancy perception inspired by human high-level visual processing.

In recent years, there has been burgeoning interest in visual-based 3D semantic perception schemes due to their relatively lower cost without compromise on performance. Initially, Bird’s Eye View (BEV) perception [4], [5], [6], [7], [8] was introduced, which significantly enhanced perceptual capabilities in autonomous driving scenarios. Subsequently, 3D semantic occupancy perception [9], [10], [11], [12], [13] emerged, extending BEV perception by a vertical dimension, thereby offering wider applicability across various scenarios. To this end, this paper focuses on visual-based 3D semantic occupancy perception and our aim is to develop a more straightforward and more efficient method for this task.

Scientists have noted in their study of human visual perception that the human brain, in high-level vision processing, tends to prioritize some objects within a scene while referencing unnoticed background information[14]. This instinct derives from humans’ need to quickly identify prey and threats during wild survival. Inspired by this, in 3D semantic occupancy perception, we imitate the mechanism of human visual perception, introducing a DETR-like[15] object detection module to guide the prediction of the 3D semantic occupancy grid. We use the bounding box results of detected objects as positional priors and the hidden features of objects as context. A spatial transformer decoder is then utilized to extract the 3D occupancy grid for each object. The "objects" we referred do not precisely denote individual objects, but rather indicate clusters of objects with the same semantics, such as a clump of trees or a group of buildings. In this way, the task of 3D semantic occupancy perception is decomposed into identifying various objects in the scene and then extracting their respective 3D occupancy grids. Object detection algorithms, from early methods like YOLO[16] to recent methods like Deformable DETR[17], have been

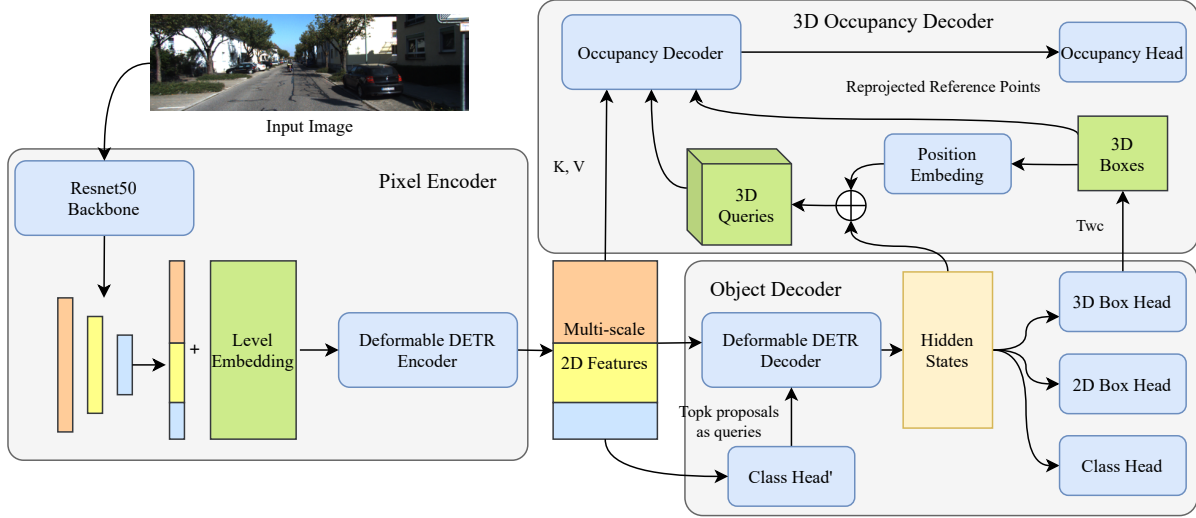


Fig. 2. The system diagram of OccupancyDETR. Arrows indicate how data flow within the system.

developed over many years, achieving excellent performance under complex scenarios. Moreover, their complexity level is significantly lower than that of 3D semantic occupancy perception. We hope to simplify 3D semantic occupancy perception methods by integrating mature object detection algorithms, aiming to make 3D semantic occupancy perception as straightforward as object detection and to unify these tasks within a single neural network. Finally, we validated our method on the SemanticKITTI dataset[18], demonstrating superior performance on smaller objects, faster speed, and less resource demand.

The main contributions of this paper are as follows:

- We propose a novel 3D semantic occupancy prediction method that incorporates object detection. This method is simple and efficient, especially adept at handling small objects, and has achieved excellent performance on the SemanticKITTI dataset.
- In response to the slow convergence problem of Detr-like algorithms, we propose an early matching pre-training. This pre-training enhances the certainty of the training and accelerates convergence.
- We have designed two types of 3D occupancy decoders—one using BEV queries with elevation, and another using 3D box queries. Through experimental comparison, we have examined the performance of these two methods on different categories of objects.

II. RELATED WORK

A. Camera-based BEV Perception

In the context of autonomous driving, employing BEV as a representation of 3D space is highly suitable, especially for scenarios involving multiple cameras mounted all around the vehicle. Numerous recent studies on BEV perception has emerged, which can be mainly categorized into two methods. The first one involves LSS and its subsequent

work[4], [19], [20], [21], which map 2D features to 3D space using depth estimated by a dedicated depth-estimation network, eventually obtaining BEV-level features through grid sampling. On the other hand, the second method is represented by BEVFormer[5], which does not require depth estimation. Instead, it treats each cell in the 3D space as a query, establishes a mapping between that cell and 2D image features by projecting it onto the image, and then updates BEV-level features using deformable attention[17].

B. 3D Semantic Scene Completion

3D semantic occupancy prediction, also known as 3D Semantic Scene Completion (SSC), has seen some novel approaches being proposed recently. One such approach involves converting 2D features into 3D space through depth prediction, as introduced in MonoScene and OccDepth[9], [10]. Another method, similar to BEVFormer, employs a query to aggregate 2D features directly in the 3D space; examples of this approach include VoxFormer, TPVFormer SurroundOcc, etc[12], [11], [22]. MonoScene[9] built the first monocular method for semantic scene completion, utilizing a 3D UNet to handle voxel features generated from line-of-sight projection. TPVFormer[11] proposed a tri-perspective view representation to describe 3D scenes. Despite its simplicity, the tri-plane format is susceptible to a deficiency of fine-grained semantic information, leading to subpar performance. OccFormer[13] uses a dual-path transformer network, decomposing the heavy 3D processing into local and global transformer pathways along the horizontal plane. In this paper, we propose using object detection information as a prior for 3D semantic occupancy prediction.

C. Mask classification-based method

Image semantic segmentation has traditionally been addressed as a per-pixel classification task. However, Max-Deeplab and MaskFormer approach semantic segmenta-

tion as a mask classification task[23], [24]. This not only naturally links semantic-level segmentation with instance-level segmentation but also yields better results in semantic segmentation compared to per-pixel classification methods. Inspired by this perspective, our study models 3D occupancy prediction as a mask classification problem.

III. APPROACH

A. Overview

An overview of our system is shown in Fig.2 and it generally consists of two parts—object detection module and 3D occupancy decoder. For a input image, we initially employ the ResNet50 backbone[25] to extract features, followed by passing these multi-scale features into a deformable encoder for further encoding. In the second step, a fixed number of queries are decoded via a deformable DETR decoder before being passed on to three heads—classification head, 2D box head, and 3D box head. The results from the classification head and 2D box head are conventional results in object detection, with objects of high confidence being selected according to the classification head’s output. In the third step, 3D Boxes of these high-confidence objects serves as the position prior of each object for the 3D occupancy decoder, providing position embeddings. The features obtained from the deformable DETR decoder serve as the context. Following this, the 3D occupancy decoder predicts the 3D occupancy grid for each object based on the multi-scale features encoded by the deformable DETR encoder.

B. Object Detection Module

In our work, we introduce object detection into 3D semantic occupancy prediction, aiming to simplifying and assisting the 3D semantic occupancy prediction. Thus, the "object" identified are different from those in conventional object detection. When generating annotated data, we first cluster semantic objects from the voxel grid based on distance, without precisely distinguishing each object. Each clustered object is then projected onto the 2D image and 2D bounding boxes is computed based on these projection points. Indeed, we consider occlusion during the projection process. We prevent completely occluded unobservable objects from affecting model learning, hence such objects are excluded. Yet, to endow the model with scene completion capabilities, partially occluded objects are preserved.

We made improvements based on the two-stage Deformable DETR, as shown in Fig.3. As the first end-to-end method based on transformers, DETR[15] is considered a new direction for object detection by many scholars due to its independence from any manual design. However, the unclear queries in DETR and the uncertainties brought by bipartite matching cause the convergence extremely slow during training. We found that during the prolonged training of DETR, most of the time, bipartite matching remains unstable. We attribute this to the fact that the model has to go through numerous of trials to find appropriate queries for the whole dataset, which takes up most of the training time. Hence,

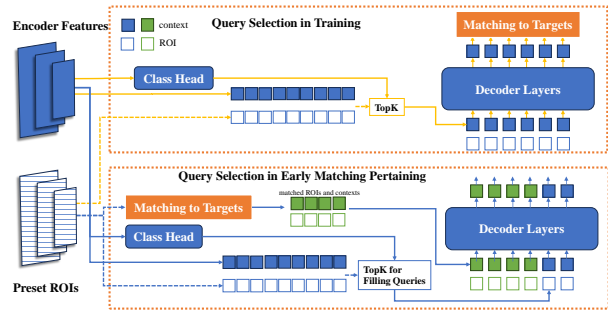


Fig. 3. Data flow diagram of the object detection module, with yellow and blue arrows representing the data flows in training and early matching pretraining respectively.

in the object detection module, we adopt the two-stage deformable DETR and designed an early matching pretraining for the query selection process. During the regular training phase, each multi-scale feature output from the encoder is assigned a preset ROI in the query selection process. These features are computed through a classification head, and the top k features with the highest scores are selected as the context of queries, with their corresponding ROIs acting as the position of queries. After passing through the deformable decoder, they are then matched with groundtruth. In the early matching pretraining, the preceding bipartite matching between the preset ROIs and groundtruth ensures certainty, avoiding the prolonged process of searching suitable queries, thereby accelerating the following regular training.

In the final stage of object detection, the queries processed by the deformable detr decoder already have vague 3D spatial information. Therefore, in addition to the classification head and 2D bounding box head, we add an extra 3D bounding box head. This is used to predict the 3D bounding box of the object in the camera coordinate system. Then, according to the camera extrinsic, it is transformed into the occupancy grid coordinate system to provide position priors for the subsequent 3D Occupancy decoder.

C. 3D Occupancy Decoder

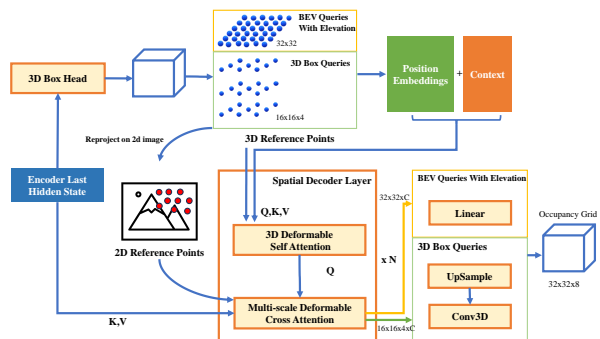


Fig. 4. Data flow diagram of the 3D occupancy decoder. There are two different query construction modes: BEV queries with elevation and 3D box queries. They differ in the stages of constructing 3D reference points and occupancy prediction.

TABLE I
SEMANTIC SCENE COMPLETION RESULT ON SEMANTICKITTI VALIDATION SET.

Method	SSC																				mIoU
	car (3.92%)	bicycle (0.03%)	motorcycle (0.05%)	truck (0.16%)	other-vehicle (0.20%)	person (0.07%)	bicyclist (0.07%)	motorcyclist (0.05%)	road (15.30%)	parking (11.12%)	sidewalk (11.13%)	other-ground (0.56%)	building (14.1%)	fence (3.90%)	vegetation (39.3%)	trunk (0.16%)	terrain (9.17%)	pole (0.29%)	traffic-sign (0.08%)		
MonoScene	23.26	0.61	0.45	6.98	1.48	1.86	1.20	0.0	56.52	14.27	26.72	0.46	14.09	5.84	17.89	2.81	29.64	4.14	2.25	11.08	
TPVFormer	23.81	0.36	0.05	8.08	4.35	0.51	0.89	0.0	56.5	20.6	25.87	0.85	13.88	5.94	16.92	2.26	30.38	3.14	1.52	11.36	
OccFormer	25.09	0.81	1.19	25.53	8.52	2.78	2.82	0.0	58.85	19.61	26.88	0.31	14.4	5.61	19.63	3.93	32.62	4.26	2.86	13.46	
OccupancyDETR-BEV	28.21	18.79	19.56	25.14	21.30	25.03	29.24	19.20	36.68	32.23	22.35	24.98	22.63	15.40	31.12	15.42	36.16	7.59	11.13	23.27	
OccupancyDETR-3D	25.55	19.84	18.81	24.42	20.84	22.62	24.16	16.47	26.80	26.76	15.27	19.28	19.72	14.34	25.40	14.89	28.87	7.13	10.39	20.08	

Following the object detection phase, high-confidence results are selected, and their features, along with the predicted 3D boxes in the occupancy grid coordinate system, are forwarded into the 3D occupancy decoder module. Given that we do not fully trust the predicted results of the 3D boxes, we modestly enlarge all of the 3D boxes. As depicted in Fig.4, we employ two query construction modes. In the BEV queries with elevation mode, we uniformly sample 32×32 points in the middle layer of this 3D box. On the other hand, in the 3D Box Queries mode, we uniformly sample $16 \times 16 \times 4$ points throughout the entire 3D box space. These points are referred to as 3D reference points. When projected onto a 2D image, they are known as 2D reference points. The position embeddings of these 3D Reference Points combined with context serve as 3D queries.

The 3D occupancy decoder comprises N layers of spatial decoder Layers. Each spatial decoder layer is constituted by a 3D deformable self attention and a multi-scale deformable cross attention. The process of 3D deformable self attention can be formulated as follows:

$$\text{DeformAttn3D}(\mathbf{z}_q, \mathbf{p}_q^{3d}, \mathbf{x}) = \sum_{m=1}^M \mathbf{W}_m \left[\sum_{k=1}^K A_{mqk} \cdot \mathbf{W}'_m \mathbf{x}(\mathbf{p}_q^{3d} + \Delta \mathbf{p}_{mqk}^{3d}) \right] \quad (1)$$

where m indexes the attention head, k indexes the sampled keys, and K is the total sampled key number. $\mathbf{p}_q^{3d} \in \mathbb{R}^3$, $\Delta \mathbf{p}_{mqk}^{3d} \in \mathbb{R}^3$ and A_{mqk} denote 3D reference points, the sampling offset and attention weight of the k^{th} sampling point in the m^{th} attention head, respectively. The process of multi-scale deformable cross attention deployed here aligns with that utilized in Deformable DETR decoder[17].

Finally, we employ a linear layer to directly elevate the BEV queries with elevation into a 3D occupancy grid. Alternatively, by using upsampling combined with 3D convolution, we expand the 3D Box Queries to the same sized 3D occupancy grid.

D. Training strategy

The entire training process is divided into four steps. Despite the multiple stages, the same annotated data is used

throughout, making the procedure not overly complicated. The first step involves pre-training through early matching to accelerate the convergence of the two-stage deformable detr. The second step involves regular training of the two-stage deformable detr, resulting in a well-trained object detection model. In the third step, the weights of the object detection model are frozen, and its results are utilized to train the 3D occupancy decoder. In the fourth and final step, the weights of the object detection model are no longer frozen, and the entire model is fine-tuned using a smaller learning rate.

Loss Function The classification loss \mathcal{L}_{cls} and the 2D bounding box loss (\mathcal{L}_{box2d} , \mathcal{L}_{giou2d}) are in accordance with the DETR[15]. The 3D bounding box loss is composed of L1 loss \mathcal{L}_{box3d} and 3D Generalized Intersection over Union (GIoU) loss \mathcal{L}_{giou3d} . The following outlines the process of computing the loss for 3D occupancy prediction. We uniformly map the occupancy grid $Occ_{gt_box}^{gt}$ within each object's 3D bounding box to a fixed $32 \times 32 \times 8$ occupancy grid. This is then restored back into the occupancy grid Occ_{scene}^{gt} of the entire scene according to the groundtruth of the 3D bounding box. Subsequently, we extract the occupancy grid $Occ_{pred_box}^{gt}$ within the predicted 3D bounding box from Occ_{scene}^{gt} , standardize it to a fixed $32 \times 32 \times 8$, and calculate the Dice loss \mathcal{L}_{dice} between $Occ_{pred_box}^{gt}$ and $Occ_{pred_box}^{pred}$. Finally, we assign different weights to various losses. The overall training objective is

$$\mathcal{L} = \mathcal{L}_{cls} + \lambda_{box2d} \mathcal{L}_{box2d} + \lambda_{giou2d} \mathcal{L}_{giou2d} + \lambda_{box3d} \mathcal{L}_{box3d} + \lambda_{giou3d} \mathcal{L}_{giou3d} + \lambda_{dice} \mathcal{L}_{dice} \quad (2)$$

IV. EXPERIMENTS

A. Datasets

The SemanticKITTI dataset[18], built upon the widely popular KITTI Odometry dataset[26], emphasizes on semantic understanding of scenes using LiDAR points and forward-facing cameras. OccupancyDETR, functioning as a monocular 3D semantic occupancy perception, employs only the left front-view camera as input. Within this dataset, the annotated semantic occupancy is represented as a voxel grid with a shape of $256 \times 256 \times 32$. Each voxel measures $0.2m \times 0.2m \times 0.2m$ and carries labels for 21 semantic categories (19 semantics, 1 free, 1 unknown). Considering that the

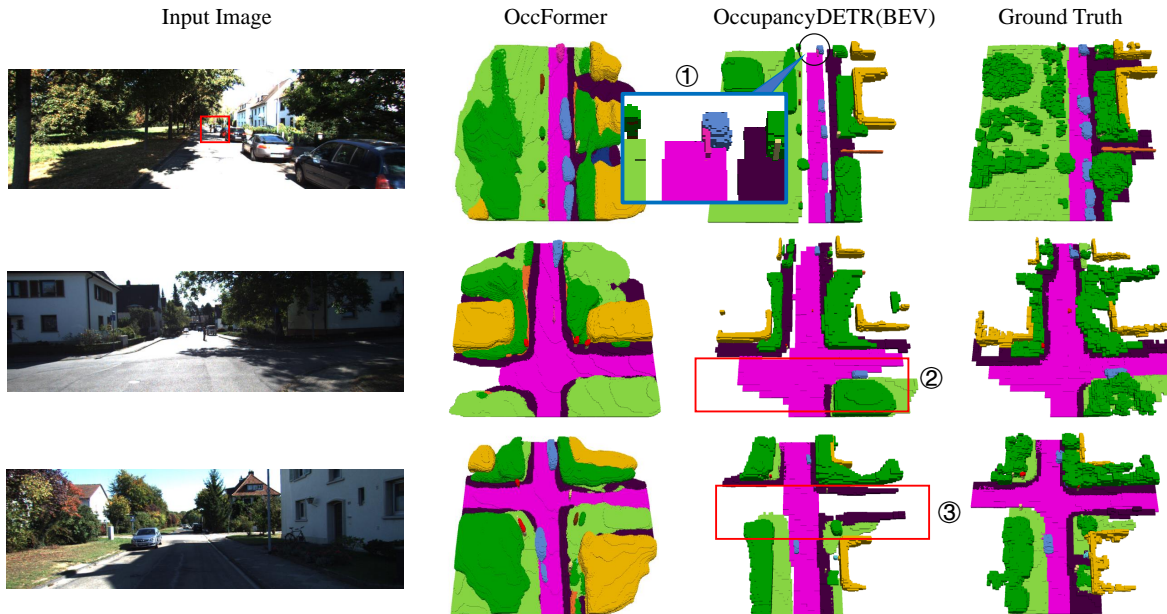
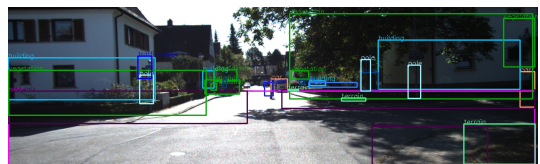
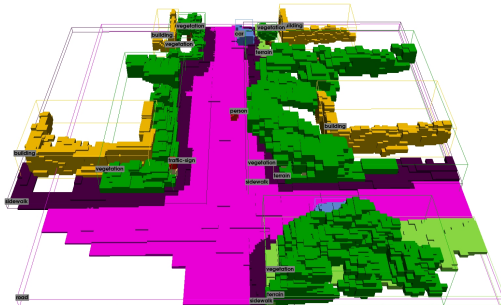


Fig. 5. Qualitative results on SemanticKITTI validation set.



(a) 2D labels



(b) 3D labels

Fig. 6. Examples of 2D and 3D labels obtained after object extraction.

semantic voxel grid of this dataset is generated from multiple frames stitched LiDAR point cloud and images, there exist gaps at distant or occluded areas. This situation hampers the clustering and extraction of objects. Consequently, we have rectified this issue by interpolation to fill in these missing cell in the semantic voxel grid. The 2D and 3D labels of the dataset obtained after object extraction are shown in Fig.6.

B. Experiments Setup

The model training is conducted on a Nvidia RTX 3090 GPU (24G), while evaluation is conducted on a Nvidia RTX 3080 GPU (16G). The training process span four stages, with respective epochs of 50 epochs, 10 epochs, 50 epochs and 10 epochs. The initial learning rates for each stage are set as $1e-4$, $2e-5$, $1e-4$, and $2e-5$ respectively, and then linearly decrease to zero. AdamW with weight decay 0.01 is employed as the optimizer. The ResNet50 backbone is initialized using a pre-trained model provided by timm[27]. Our experimental objective is to validate the feasibility and traits of this new framework; thus, we do not use any data augmentation.

C. Main Results

As shown in Table I, we report the mean intersection over union (mIoU) for semantic scene completion (SSC) task. We compare our method with other monocular 3D semantic occupancy perception methods and analyze the results. As can be seen, our method significantly outperforms others on small targets, which is attributed to the object detection task; however, in categories such as roads and sidewalks, our method falls behind others, for which we have conducted further analysis. The representative cases of our analysis are illustrated in Fig.5. ① shows the performance of our method on small object categories, which can detect a bicyclist at a distance. ② and ③ reveal the reasons for the poor performance of our method on the 'road' and 'sidewalk' categories. We think that this is due to the fact that our method first detects objects, then predicts the 3D occupancy grid for each object. However, the ability to extract features regarding

TABLE II
MODEL PARAMETERS AND SINGLE IMAGE INFERENCE TIME ON
SEMANTICKITTI VALIDATION SET.

Method	Parameters	Inference Time
MonoScene	149.55M	789ms
TPVFormer	140.55M	518ms
OccFormer	203.68M	415ms
OccupancyDETR-BEV	46.89M	174ms
OccupancyDETR-3D	48.78M	210ms

the relationships between different objects in 3D space is relatively weak. This leads to the phenomenon where our model can directly detect nearby crossroads based on image, but fails to indirectly complete distant crossroads based on other 3D objects.

Despite this, the advantage of our method in terms of speed and resource requirements is significant. The inference time pre frame and parameter count of our method are shown in Table II. Our method has an average inference time of 174ms (on Nvidia RTX 3080), which has already achieved real-time performance.

Next, we compare the two modes of BEV queries with elevation and 3D box queries. We find that for most categories, the BEV queries with elevation mode perform better, especially in the four categories of road, sidewalk, terrain, and vegetation, where there is a noticeable difference. Considering that these four categories are typically flat in this dataset, they are more suitable for the BEV queries with elevation mode. This illustrates the significant performance differences between these two modes for objects with different shapes.

D. Comparative Study on Early Matching Pretraining

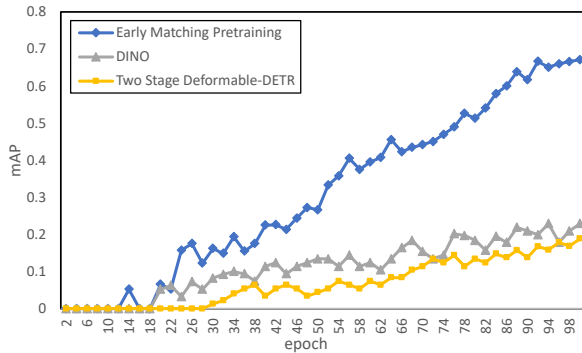


Fig. 7. Training convergence curves evaluated on SemanticKITTI for early matching pretraining, DINO and two stage Deformable DETR.

In order to validate the positive impact of early matching pretraining on the training of DETR-like [15] object detection models, we conduct a comparative study under the same experimental conditions between DINO[28] and two stage Deformable DETR[17]. In our experiment, we set the initial learning rate at $1e-4$ and decrease it linearly to zero within 100 epochs. Fig.7 illustrates the mAP curves for the

three methods on the validation set during training, showing that early matching pretraining leads to faster convergence in training. Furthermore, we analyze DINO’s performance, which is a method based on the two stage Deformable DETR. Several improvements are proposed by DINO to accelerate convergence, one of which is mixed query selection. This process involves using learnable embeddings as static content queries while selecting anchors through query selection to serve as dynamic anchors. However, a misalignment issue exists between the orders of static content queries and dynamic anchors. We hypothesize that this discrepancy is the reason DINO’s performance does not meet expectations.

V. CONCLUSIONS

In this paper, we propose for the first time a method of 3D semantic occupancy perception combined with object detection. Utilizing object detection simplifies the task of 3D occupancy perception, reducing the resources needed by the algorithm and increasing its speed, while significantly enhancing performance on small objects. Through experiments on the SemanticKITTI dataset, our method has demonstrated commendable performance, attesting to the efficiency and simplicity of our framework. However, due to the lack of correlation between different objects in 3D space, our method does not perform well in a few case. In future work, we plan to enhance this framework’s ability to extract the features between different objects in 3D space, and intend to extend with multiple frame input.

REFERENCES

- [1] G. P. Meyer, J. Charland, D. Hegde, A. Laddha, and C. Vallespi-Gonzalez, “Sensor fusion for joint 3d object detection and semantic segmentation,” in *IEEE Conference on Computer Vision and Pattern Recognition Workshops, CVPR Workshops 2019, Long Beach, CA, USA, June 16-20, 2019*. Computer Vision Foundation / IEEE, 2019, pp. 1230–1237. [Online]. Available: http://openaccess.thecvf.com/content_CVPRW_2019/html/WAD/Meyer_Sensor_Fusion_for_Joint_3D_Object_Detection_and_Semantic_Segmentation_CVPRW_2019_paper.html
- [2] D. Xu, D. Anguelov, and A. Jain, “Pointfusion: Deep sensor fusion for 3d bounding box estimation,” in *2018 IEEE Conference on Computer Vision and Pattern Recognition, CVPR 2018, Salt Lake City, UT, USA, June 18-22, 2018*. Computer Vision Foundation / IEEE Computer Society, 2018, pp. 244–253. [Online]. Available: http://openaccess.thecvf.com/content_cvpr_2018/html/Xu_PointFusion_Deep_Sensor_CVPR_2018_paper.html
- [3] V. A. Sindagi, Y. Zhou, and O. Tuzel, “Mvx-net: Multimodal voxelnet for 3d object detection,” in *International Conference on Robotics and Automation, ICRA 2019, Montreal, QC, Canada, May 20-24, 2019*. IEEE, 2019, pp. 7276–7282. [Online]. Available: <https://doi.org/10.1109/ICRA.2019.8794195>
- [4] J. Philion and S. Fidler, “Lift, splat, shoot: Encoding images from arbitrary camera rigs by implicitly unprojecting to 3d,” in *Computer Vision - ECCV 2020 - 16th European Conference, Glasgow, UK, August 23-28, 2020, Proceedings, Part XIV*, ser. Lecture Notes in Computer Science, A. Vedaldi, H. Bischof, T. Brox, and J. Frahm, Eds., vol. 12359. Springer, 2020, pp. 194–210. [Online]. Available: https://doi.org/10.1007/978-3-030-58568-6_12
- [5] Z. Li, W. Wang, H. Li, E. Xie, C. Sima, T. Lu, Y. Qiao, and J. Dai, “Bevformer: Learning bird’s-eye-view representation from multi-camera images via spatiotemporal transformers,” in *Computer Vision - ECCV 2022 - 17th European Conference, Tel Aviv, Israel, October 23-27, 2022, Proceedings, Part IX*, ser. Lecture Notes in Computer Science, S. Avidan, G. J. Brostow, M. Cissé, G. M. Farinella, and T. Hassner, Eds., vol. 13669. Springer, 2022, pp. 1–18. [Online]. Available: https://doi.org/10.1007/978-3-031-20077-9_1

- [6] J. Huang, G. Huang, Z. Zhu, and D. Du, "Bevdet: High-performance multi-camera 3d object detection in bird-eye-view," *CoRR*, vol. abs/2112.11790, 2021. [Online]. Available: <https://arxiv.org/abs/2112.11790>
- [7] Q. Li, Y. Wang, Y. Wang, and H. Zhao, "Hdmapnet: An online HD map construction and evaluation framework," in *2022 International Conference on Robotics and Automation, ICRA 2022, Philadelphia, PA, USA, May 23-27, 2022*. IEEE, 2022, pp. 4628–4634. [Online]. Available: <https://doi.org/10.1109/ICRA46639.2022.9812383>
- [8] B. Liao, S. Chen, X. Wang, T. Cheng, Q. Zhang, W. Liu, and C. Huang, "Maptr: Structured modeling and learning for online vectorized HD map construction," in *The Eleventh International Conference on Learning Representations, ICLR 2023, Kigali, Rwanda, May 1-5, 2023*. OpenReview.net, 2023. [Online]. Available: https://openreview.net/pdf?id=k7p_YAO7yE
- [9] A. Cao and R. de Charette, "Monoscene: Monocular 3d semantic scene completion," in *IEEE/CVF Conference on Computer Vision and Pattern Recognition, CVPR 2022, New Orleans, LA, USA, June 18-24, 2022*. IEEE, 2022, pp. 3981–3991. [Online]. Available: <https://doi.org/10.1109/CVPR52688.2022.00396>
- [10] R. Miao, W. Liu, M. Chen, Z. Gong, W. Xu, C. Hu, and S. Zhou, "Occdepth: A depth-aware method for 3d semantic scene completion," *CoRR*, vol. abs/2302.13540, 2023. [Online]. Available: <https://doi.org/10.48550/arXiv.2302.13540>
- [11] Y. Huang, W. Zheng, Y. Zhang, J. Zhou, and J. Lu, "Tri-perspective view for vision-based 3d semantic occupancy prediction," *CoRR*, vol. abs/2302.07817, 2023. [Online]. Available: <https://doi.org/10.48550/arXiv.2302.07817>
- [12] Y. Li, Z. Yu, C. B. Choy, C. Xiao, J. M. Álvarez, S. Fidler, C. Feng, and A. Anandkumar, "Voxformer: Sparse voxel transformer for camera-based 3d semantic scene completion," *CoRR*, vol. abs/2302.12251, 2023. [Online]. Available: <https://doi.org/10.48550/arXiv.2302.12251>
- [13] Y. Zhang, Z. Zhu, and D. Du, "Occformer: Dual-path transformer for vision-based 3d semantic occupancy prediction," *CoRR*, vol. abs/2304.05316, 2023. [Online]. Available: <https://doi.org/10.48550/arXiv.2304.05316>
- [14] E. R. Kandel, J. H. Schwartz, T. M. Jessell, S. Siegelbaum, A. J. Hudspeth, S. Mack, et al., *Principles of neural science*. McGraw-hill New York, 2000, vol. 4.
- [15] N. Carion, F. Massa, G. Synnaeve, N. Usunier, A. Kirillov, and S. Zagoruyko, "End-to-end object detection with transformers," in *Computer Vision - ECCV 2020 - 16th European Conference, Glasgow, UK, August 23-28, 2020, Proceedings, Part I*, ser. Lecture Notes in Computer Science, A. Vedaldi, H. Bischof, T. Brox, and J. Frahm, Eds., vol. 12346. Springer, 2020, pp. 213–229. [Online]. Available: https://doi.org/10.1007/978-3-030-58452-8_13
- [16] J. Redmon, S. K. Divvala, R. B. Girshick, and A. Farhadi, "You only look once: Unified, real-time object detection," in *2016 IEEE Conference on Computer Vision and Pattern Recognition, CVPR 2016, Las Vegas, NV, USA, June 27-30, 2016*. IEEE Computer Society, 2016, pp. 779–788. [Online]. Available: <https://doi.org/10.1109/CVPR.2016.91>
- [17] X. Zhu, W. Su, L. Lu, B. Li, X. Wang, and J. Dai, "Deformable DETR: deformable transformers for end-to-end object detection," in *9th International Conference on Learning Representations, ICLR 2021, Virtual Event, Austria, May 3-7, 2021*. OpenReview.net, 2021. [Online]. Available: <https://openreview.net/forum?id=gZ9hCDWe6ke>
- [18] J. Behley, M. Garbade, A. Milioto, J. Quenzel, S. Behnke, C. Stachniss, and J. Gall, "Semantickitti: A dataset for semantic scene understanding of lidar sequences," in *2019 IEEE/CVF International Conference on Computer Vision, ICCV 2019, Seoul, Korea (South), October 27 - November 2, 2019*. IEEE, 2019, pp. 9296–9306. [Online]. Available: <https://doi.org/10.1109/ICCV.2019.00939>
- [19] C. Reading, A. Harakeh, J. Chae, and S. L. Waslander, "Categorical depth distribution network for monocular 3d object detection," in *IEEE Conference on Computer Vision and Pattern Recognition, CVPR 2021, virtual, June 19-25, 2021*. Computer Vision Foundation / IEEE, 2021, pp. 8555–8564. [Online]. Available: https://openaccess.thecvf.com/content/CVPR2021/html/Reading_Categorical_Depth_Distribution_Network_for_Monocular_3D_Object_Detection_CVPR_2021_paper.html
- [20] Y. Li, Z. Ge, G. Yu, J. Yang, Z. Wang, Y. Shi, J. Sun, and Z. Li, "Bevdepth: Acquisition of reliable depth for multi-view 3d object detection," in *Thirty-Seventh AAAI Conference on Artificial Intelligence, AAAI 2023, Thirty-Fifth Conference on Innovative Applications of Artificial Intelligence, IAAI 2023, Thirteenth Symposium on Educational Advances in Artificial Intelligence, EAAI 2023, Washington, DC, USA, February 7-14, 2023*, B. Williams, Y. Chen, and J. Neville, Eds. AAAI Press, 2023, pp. 1477–1485. [Online]. Available: <https://ojs.aaai.org/index.php/AAAI/article/view/25233>
- [21] A. Hu, Z. Murez, N. Mohan, S. Dudas, J. Hawke, V. Badrinarayanan, R. Cipolla, and A. Kendall, "FIERY: future instance prediction in bird's-eye view from surround monocular cameras," in *2021 IEEE/CVF International Conference on Computer Vision, ICCV 2021, Montreal, QC, Canada, October 10-17, 2021*. IEEE, 2021, pp. 15 253–15 262. [Online]. Available: <https://doi.org/10.1109/ICCV48922.2021.01499>
- [22] Y. Wei, L. Zhao, W. Zheng, Z. Zhu, J. Zhou, and J. Lu, "Surroundocc: Multi-camera 3d occupancy prediction for autonomous driving," *CoRR*, vol. abs/2303.09551, 2023. [Online]. Available: <https://doi.org/10.48550/arXiv.2303.09551>
- [23] H. Wang, Y. Zhu, H. Adam, A. L. Yuille, and L. Chen, "Max-deeplab: End-to-end panoptic segmentation with mask transformers," in *IEEE Conference on Computer Vision and Pattern Recognition, CVPR 2021, virtual, June 19-25, 2021*. Computer Vision Foundation / IEEE, 2021, pp. 5463–5474. [Online]. Available: https://openaccess.thecvf.com/content/CVPR2021/html/Wang_Max-DeepLab_End-to-End_Panoptic_Segmentation_With_Mask_Transformers_CVPR_2021_paper.html
- [24] Z. Li, J. Yang, B. Wang, Y. Li, and T. Pan, "Maskformer with improved encoder-decoder module for semantic segmentation of fine-resolution remote sensing images," in *2022 IEEE International Conference on Image Processing, ICIP 2022, Bordeaux, France, 16-19 October 2022*. IEEE, 2022, pp. 1971–1975. [Online]. Available: <https://doi.org/10.1109/ICIP46576.2022.9897888>
- [25] K. He, X. Zhang, S. Ren, and J. Sun, "Deep residual learning for image recognition," in *2016 IEEE Conference on Computer Vision and Pattern Recognition, CVPR 2016, Las Vegas, NV, USA, June 27-30, 2016*. IEEE Computer Society, 2016, pp. 770–778. [Online]. Available: <https://doi.org/10.1109/CVPR.2016.90>
- [26] A. Geiger, P. Lenz, and R. Urtasun, "Are we ready for autonomous driving? the KITTI vision benchmark suite," in *2012 IEEE Conference on Computer Vision and Pattern Recognition, Providence, RI, USA, June 16-21, 2012*. IEEE Computer Society, 2012, pp. 3354–3361. [Online]. Available: <https://doi.org/10.1109/CVPR.2012.6248074>
- [27] R. Wightman, H. Touvron, and H. Jégou, "Resnet strikes back: An improved training procedure in timm," *CoRR*, vol. abs/2110.00476, 2021. [Online]. Available: <https://arxiv.org/abs/2110.00476>
- [28] H. Zhang, F. Li, S. Liu, L. Zhang, H. Su, J. Zhu, L. M. Ni, and H. Shum, "DINO: DETR with improved denoising anchor boxes for end-to-end object detection," in *The Eleventh International Conference on Learning Representations, ICLR 2023, Kigali, Rwanda, May 1-5, 2023*. OpenReview.net, 2023. [Online]. Available: <https://openreview.net/pdf?id=3mRwyG5one>